ORIGINAL PAPER

Chemical, electrochemical, thermodynamic and adsorption study of EN8 dual-phase steel with ferrite-martensite structure in 0.5 M H$_2$SO$_4$ using pectin as inhibitor

P. R. Prabhu[1] · Pavan Hiremath[1] · Deepa Prabhu[2] · M. C. Gowrishankar[1] · B. M. Gurumurthy[1]

Abstract

This paper presents the corrosion and inhibition behavior of heat-treated EN8 dual-phase steel with ferrite-martensite structure with pectin in 0.5 M sulphuric acid. The corrosion studies were performed using the weight loss method, electrochemical techniques such as potentiodynamic polarization measurements, and impedance spectroscopy. The study was done at different concentrations of pectin in the temperature range of 40 to 70 °C and immersion time of 1, 3, 5, and 7 h. The results showed that the inhibition performance of pectin has enhanced with an increase in pectin concentration and decreased with the temperature and time of exposure. From the weight loss study, highest inhibition efficiency of 76.43% was achieved at 5.0 g/L at 1 h of exposure at 40 °C. The maximum inhibition efficiency of 62% was obtained with 5.0 g/L of pectin at 40 °C by potentiodynamic polarization method. The energy, enthalpy, and entropy of activation and also thermodynamic parameters like free energy, enthalpy, and entropy of adsorption were assessed and discussed. Appropriate adsorption isotherm was fit to the obtained experimental outcomes and achieved Langmuir adsorption isotherm to be the best fit and obeyed physical adsorption. Surface analysis: scanning electron microscopy, X-ray diffraction techniques, atomic force microscopy, and energy dispersive X-ray were done with and without the addition of pectin. The metal surface appears to be uniform and smooth in the presence of pectin and adsorption was confirmed by surface analysis.

Keywords EN8 steel · Heat treatment · Ferrite-martensite · Sulphuric acid medium · Weight loss method · Electrochemical studies

Introduction

Heat treatment is a process used to modify the properties of a material. Here, the metal is heated and then cooled at the desired temperature, to attain the desired microstructure. EN8 steel is plain medium carbon steel with moderate strength in an as-cast state and possible to modify the properties in a wider range. It is the most commonly used type of steel, usually used in the normalized condition. This steel can be utilized for the manufacturing of automobile parts such as axle shaft, gear shaft, bolts, and studs. Dual-phase (DP) steels have received massive consideration in the past few decades because of increased application in the automotive industry. When compared to conventional high strength low alloyed (HSLA) steels, DP steels display improved mechanical properties (Abedini et al. 2019; Salamci et al. 2017). Steels with DP structure have a place with a gathering of present-day multi-phase steels described by ferrite matrix containing at least one or more phases (martensite, bainite, and leftover austenite) (Abedini et al. 2019; Gerengi et al. 2020; Keleştemur et al. 2009; Song et al. 2019). The concurrence of delicate/hard phases and their connection in working conditions permit both high strength and malleability to be accomplished. DP steels comprising of delicate ferrite and hard martensite show better mechanical properties looked at than regular HSLA steels (Abedini et al. 2019; Song et al. 2020). That has driven the specialists to investigate their appropriateness for various structural and constructional purposes (Katiyar et al. 2019). Though

✉ Deepa Prabhu
  deepa.prabhu@manipal.edu

[1] Department of Mechanical and Manufacturing Engineering, Manipal Institute of Technology, Manipal Academy of Higher Education, Manipal, Karnataka 576104, India

[2] Department of Chemistry, International Center for Applied Sciences, Manipal Academy of Higher Education, Manipal, Karnataka 576104, India

plenty of research articles were published concerning a generally excellent blend of mechanical properties in DP steels (Karimi et al. 2017; Basantia et al. 2021; Bilal et al. 2019; Fereiduni and Ghasemi Banadkouki 2014; Kumar et al. 2019; Shahzad et al. 2018; Xiong et al. 2019; Zhao et al. 2019; Zhu 2019), further examinations are important to discover the impact of phase constituents on the corrosion resistance properties (Bignozzi et al. 2020; Gürkan Aydın 2019; Ma et al. 2020; Prabhu et al. 2020a, b; Zhang et al. 2020).

Corrosion of metals is an issue that needs to be resolved. Deterioration of chemical plants, equipment, or disaster due to corrosion had been widely reported. The study of carbon steel corrosion in several corrosive conditions is very important. Even though there is the development of new corrosion-resistant alloys, carbon steel is still the frequently used steel because of its versatility in terms of mechanical properties, availability and economics. Corrosion inhibitors remain an important method to protect materials against the process of corrosion in a corrosive environment (Nathan 1973; Saxena et al. 2020; Shinato et al. 2020). The essential organic molecules containing heteroatom like sulfur, oxygen, nitrogen, etc., exhibit inhibiting action which is mainly referring to their adsorption on the surface of the metal (Branzoi et al. 2020; El Faydy et al. 2020; Mahgoub et al. 2010; Tabatabaei majd, 2020). Moreover, the latest development in the protection of the surface of the metal is using nontoxic inhibitors (Galo et al. 2020; Hoai et al. 2019; Hynes et al. 2021; Manssouri et al. 2021; Negm et al. 2011; Pais and Rao 2021; Şahin et al. 2020). Saxena et al. have assessed the inhibition action of *Citrus sinensis* extract on C-steel corrosion in 0.5 M H_2SO_4 (Saxena et al. 2020).

Pectin is a heteropolysaccharide predominantly extracted from citrus fruits. It has a poly (D-galacturonic acid) linked through $\alpha(1,4)$-glycosidic linkage. There has been a study of pectin on 6061Al–15%(V) SiC(P) composite in 0.025 M HCl (Charitha and Rao 2020). Pectin, with a low cost of production, soluble in sulphuric acid, was selected to act as an active inhibitor to control corrosion of EN8 steel. In the framework of our studies with environment-friendly inhibitors (Li et al. 2019; Prabhu and Rao 2019; Prabhu et al. 2020a, b) for corrosion control of EN8 steel, in the present examination, we have investigated the usefulness of pectin as an inhibitor to control the corrosion of EN8 steel in sulphuric acid medium.

Furthermore, there is general evidence that temperature is one of the important factors that may affect the performance of metals in a corrosive environment, and may also affect the interaction between the metal and the inhibitor. Also, in corrosive medium, the rate of metal dissolution increases with temperatures (Bentiss et al. 2005; Mert et al. 2011). Several investigations have been done in reviewing the inhibition of corrosion of steel in acidic medium with the influence of

temperature in the presence of eco-friendly inhibitors (Lowmunkhong et al. 2010; Obi-Egbedi et al. 2012; Prabhu and Rao 2013). Qiang et al. (2018) experimented to understand the influence of temperature on corrosion and inhibition of X70 steel by Ginkgo leaf extract in HCl solution. Solomon et al. (2010) studied the inhibition and adsorption nature of carboxymethyl cellulose on mild steel in H_2SO_4 at varying temperature.

Different measuring techniques are available to study the behavior on the steel like gravimetric, electrochemical and surface measurements. The electrochemical measurements are useful due to their high sensitivity, simple procedures and low cost (Stoica et al. 2012). The rate of the corrosion process can be obtained by weight loss method, Tafel extrapolation, impedance spectroscopy, linear polarization resistance, electrochemical noise, etc. (Berradja 2019).

The current work emphasizes the assessment of the inhibition of pectin in EN8 DP steel with ferrite-martensite (F-M) structure corrosion in 0.5 M sulphuric acid (H_2SO_4) at various temperatures, exposure time, and concentration of inhibitor. Various kinetic and thermodynamic parameters for EN8 steel corrosion with and without the use of pectin were calculated and deliberated.

Methodology

Material, medium, and inhibitor preparation

Table 1 presents the chemical composition of the EN8 steel used for the study. The heat-treated test samples were prepared in a cylindrical rod shape of 19 mm diameter and 8 mm height. The specimens were then polished with varying grades of emery papers (100–2000 μm) and followed by disk polishing with different grades (3 μm to 0.25 μm) of diamond paste. The specimens were then washed with distilled water, cleaned with acetone, and eventually desiccated before submerging it in the medium.

The medium selected for the investigation is 0.5 M sulphuric acid. The sulphuric acid solution was prepared by diluting analytical reagent-grade sulphuric acid (98%) to the appropriate volume. The solution was standardized by the

Table 1 Chemical composition of EN8 steel

Element	Composition (wt%)	Element	Composition (wt%)
C	0.247	Cr	0.095
Si	0.199	Ni	0.044
P	0.027	Cu	0.059
Mn	0.54	Mo	0.027
S	0.037	Fe	98.7

volumetric method. The corrosion tests were then performed at varying temperatures of 40, 50, 60, and 70 °C.

The inhibitor used in our experiments is pectin (commercially available). The structure of pectin is given in Fig. 1. Its main constituent is galacturonic acid that is a sugar acid (derived from galactose). The investigation was done in 0.5 M H_2SO_4 solution in the absence and presence of the pectin (0.5, 2.0, 3.5, and 5.0 g/L).

Heat treatment

Initially, the samples were heated in an electric muffle furnace at the predetermined austenitization temperature (900 °C). The process PQ (as shown in Fig. 2a) represents the austenitization process. The experimental coupons were kept at the austenitization temperature for a fixed duration of 2 h. After isothermal holding for 2 h, specimens are quickly taken out from the furnace for air cooling to get the room temperature structure. Further, austenitizing is carried out at 790 °C for 2 h followed by quenching in water to form an F-M dual-phase structure. Figure 2b shows the heat treatment procedure to obtain an F-M dual-phase structure.

Figure 3a shows the microstructure of EN8 steel in as-received conditions. The steel shows ferrite and lamellar
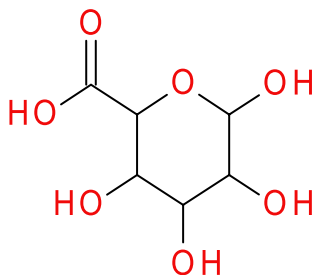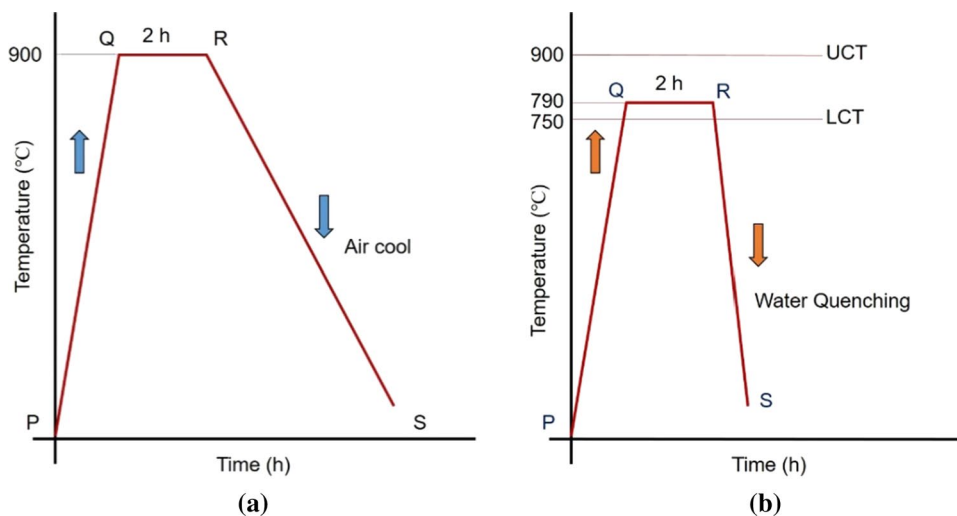
pearlite grains. The steel rods might have undergone air cooling, resulting in the formation of fine grains. Figure 3b shows the microstructure of steel in the normalized condition. The microstructure displays fine and lamellar pearlite and proeutectoid ferrite. The interlamellar distance in normalized pearlite is smaller when compared to the as-bought steel as a result of normalizing heat treatment. Fine pearlite enhances the mechanical properties of the steel. Figure 3c shows the duplex structure in the steel containing F-M. The steel is heated in between lower critical temperature (LCT) and upper critical temperature (UCT) of the iron carbide phase diagram where homogeneous austenite is not formed. During this process, the pearlite of as-received steel converts into austenite first and proeutectoid ferrite remains unchanged. When the steel is quenched from this temperature, the austenite converts to lower-temperature structures like martensite. When austenite is cooled in this temperature range, carbon atoms redistribute in austenite. Low carbon regions transform to ferrite by diffusionless processes and result in fine needles of ferrite. As time passes, carbon diffuses out and precipitates in the form of fine carbides, the arrangement of carbides here is not in the form of lamellar structure. Figure 3c shows the microstructure having ferrite and martensite. Martensite is a highly distorted structure formed because of the arrested diffusion of carbon particles from austenite. When the steel is held in the inter-critical temperatures and is quenched in liquid at room temperature, the austenite converts into martensite and proeutectoid ferrite remains unchanged. As the cooling takes place, the carbon atoms do not get enough time to diffuse out of austenite and lead to the formation of a distorted martensite structure.

Weight loss method

The measurement of weight loss of metals was studied on the EN8 steel in a circular form of size 19 mm diameter and

Fig. 1 Structure of pectin

Fig. 2 **a** Normalizing heat treatment cycle, **b** Heat treatment procedure for dual-phase F-M structure
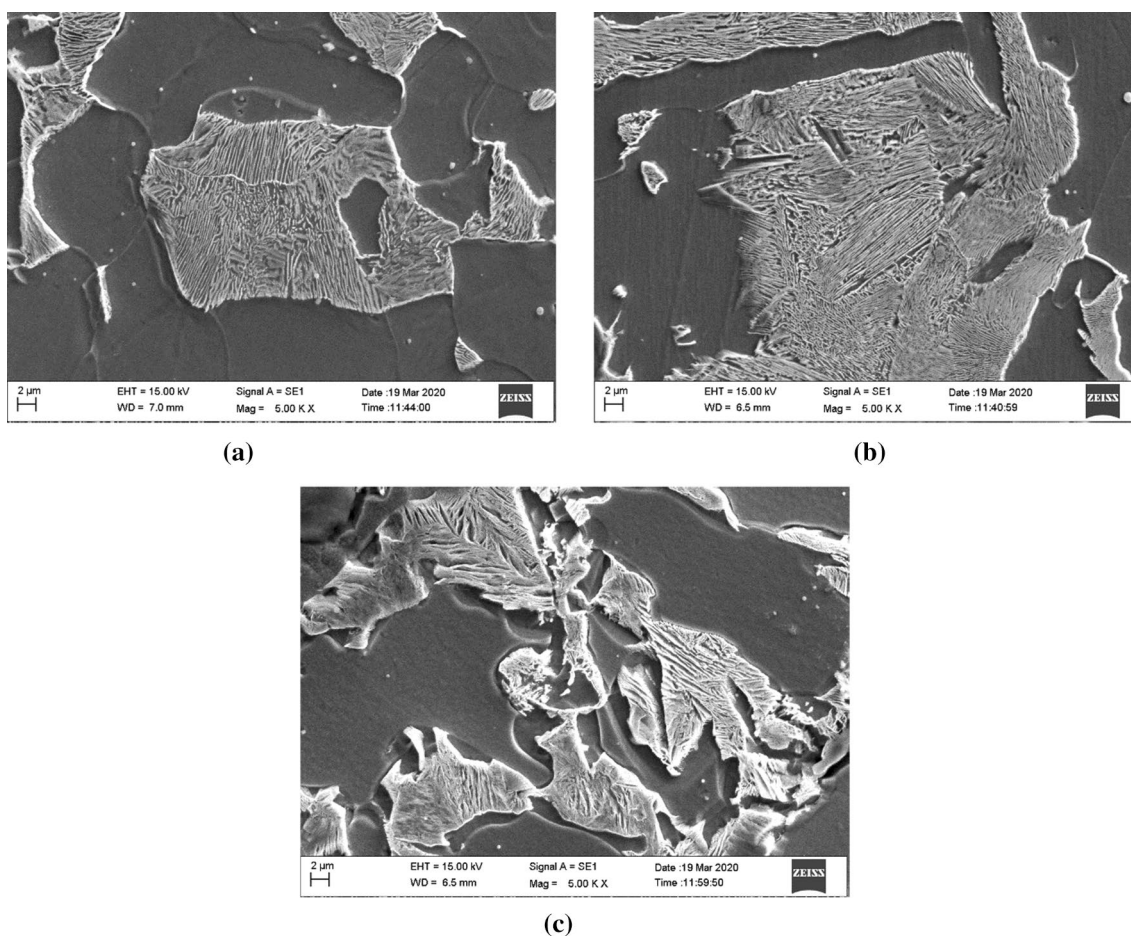
Fig. 3 SEM images of EN8 steel in different conditions. **a** As bought, **b** normalized, **c** Austenitized at 790 °C for 2 h followed by quenching in water to form DP F-M structure

8 mm height in 0.5 M H_2SO_4 solution with various concentrations of pectin. Each sample was weighed using a digital electronic balance of four decimal points and then placed in 100 ml of corrosion and inhibitor solutions. The duration of the immersion was 1, 3, 5, and 7 h at the temperature of 40, 50, 60, and 70 °C. After the exposure, the surface of the test specimens was cleaned according to the ASTM G1-90 standard procedure (A. G1-90 1999), and the weight difference (Δ_w) was calculated before and after exposure to obtain the inhibition efficiency (IE_w, %) with the help of Eq. 1 and followed by corrosion rate (CR_w) calculation using Eq. 2. The mean value of the weight loss was taken after performing the trials in triplicate.

$$IE_w(\%) = \frac{w_0 - w_i}{w_0} \times 100, \qquad (1)$$

where w_i and w_0 represent weight loss values in the presence and absence of pectin, respectively, in grams.

The corrosion rate (CR_w) of the specimen was calculated using the relation:

$$CR_w = \frac{3.45 \times 10^6 \times \Delta w}{A \times t \times d}(mpy), \qquad (2)$$

where Δ_w, weight loss (g m); A, area of the specimen exposed to acid medium (cm^2); t, the immersion time (h); and d, density of EN8 steel (g cm^{-3}).

Effect of corrosion process with temperature and calculations of activation parameters

The CR's were calculated at different temperatures (40–70 °C) by the weight loss method was applied for the determination of E_a (activation energy), $\Delta H^{\#}$ (activation enthalpy), and $\Delta S^{\#}$ (activation entropy) (Prabhu et al. 2021). The determination of each activation parameter is done as per the literature (Prabhu and Rao 2019).

Adsorption isotherm and thermodynamic parameters

The interaction of the metal surface with the pectin molecule is described by adsorption isotherm. The correlation coefficient (R^2) and best fits are the deciding criteria for selecting the suitable adsorption isotherm. The calculation of standard free energy of adsorption (ΔG°_{ads}) was obtained from the adsorption equilibrium constant (K) (Prabhu and Rao 2013; Prabhu et al. 2021). The standard enthalpy of adsorption (ΔH°_{ads}) and standard entropy of adsorption (ΔS°_{ads}) were obtained from a plot of ΔG°_{ads} vs T.

Potentiodynamic polarization (PDP) and electrochemical impedance spectroscopy (EIS)

For PDP and EIS studies the procedures were as per the literature (Prabhu et al. 2021). The specimen with a surface area of 0.5 cm^2 was taken for the study. The experiments were carried out at 40 ± 1 °C. The instrument used for performing the electrochemical measurement was model CH600E. The anodic and cathodic polarization segments were extrapolated to the corrosion potential to acquire corrosion current densities (i_{corr}). The inhibition efficiency (IE$_i$, %) was estimated from the i_{corr} values using the Eq. 3:

$$IE_i\,(\%) = \frac{i^0_{corr} - i^{inh}_{corr}}{i^0_{corr}} \times 100, \tag{3}$$

where i^0_{corr} and i^{inh}_{corr} are the corrosion current densities when pectin is absent and in the presence of pectin, respectively.

Measurements of the EIS were also performed according to the literature (Prabhu et al. 2021). Impedance charts are given in the Nyquist representation and the Bode phase and magnitude graphs. The polarization resistance values (R_p) were achieved by EIS by adding the solution resistance (R_s) and charge transfer resistance (R_{ct}). The inhibition efficiency (IE$_{EIS}$, %) of pectin was computed from Eq. 4:

$$IE_{EIS}(\%) = \frac{R^{inh}_p - R^0_p}{R^{inh}_p} \times 100, \tag{4}$$

where R^0_p and R^{inh}_p are the charge transfer resistance without and in the presence of pectin, respectively. All electrochemical measurements were performed in an aerated solution with the unstirred condition.

Surface characterization

The heat-treated samples surface analysis was done using scanning electron microscopy (SEM) at 5 K X magnification.

The surface morphology of EN8 steel immersed in 0.5 M H$_2$SO$_4$ solution with and without 5.0 g/L pectin inhibitor was investigated by capturing the images with the magnification of 1 K X using EVO MA18 for SEM and energy dispersive X-ray (EDX). IB342 Innova model was used for capturing atomic force microscopy (AFM) spectral images. Using Miniflex 600 model instruments, the X-ray diffraction (XRD) images were obtained. All the surface characterization was carried out on the surface of corroded (EN8 steel + 0.5 M H$_2$SO$_4$) and inhibited surfaces (EN8 steel + 0.5 M H$_2$SO$_4$ + 5.0 g/L).

Result and discussion

Weight loss method

Figure 4 represents the effect of weight loss of EN8 DP steel with F-M structure in 0.5 M H$_2$SO$_4$ solution at various temperatures and at various time intervals. It is observed that weight loss increased with increasing time of exposure as well as with an increase in temperature suggesting the enhanced corrosiveness of the metal on prolonged exposure to acid medium due to hydrolytic degradation. Figure 4 represents the weight loss data of EN8 steel in 0.5 M H$_2$SO$_4$ solution. Figure 5 reflects the weight loss data of EN8 steel in 0.5 M H$_2$SO$_4$ solution in the presence of pectin with various concentrations and at different temperatures. Increased pectin concentration increases the inhibition effectiveness EI$_w$% to approximately 76.43% at 5.0 g/L at 1 h of exposure at 40 °C. The EI$_w$% is attributed to the adsorption of pectin over the EN8 steel specimen surface. This adsorption confines the degradation of metals and therefore reduces weight
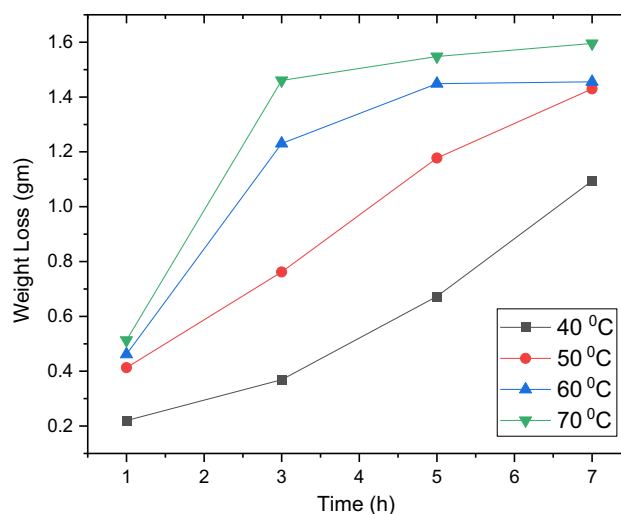
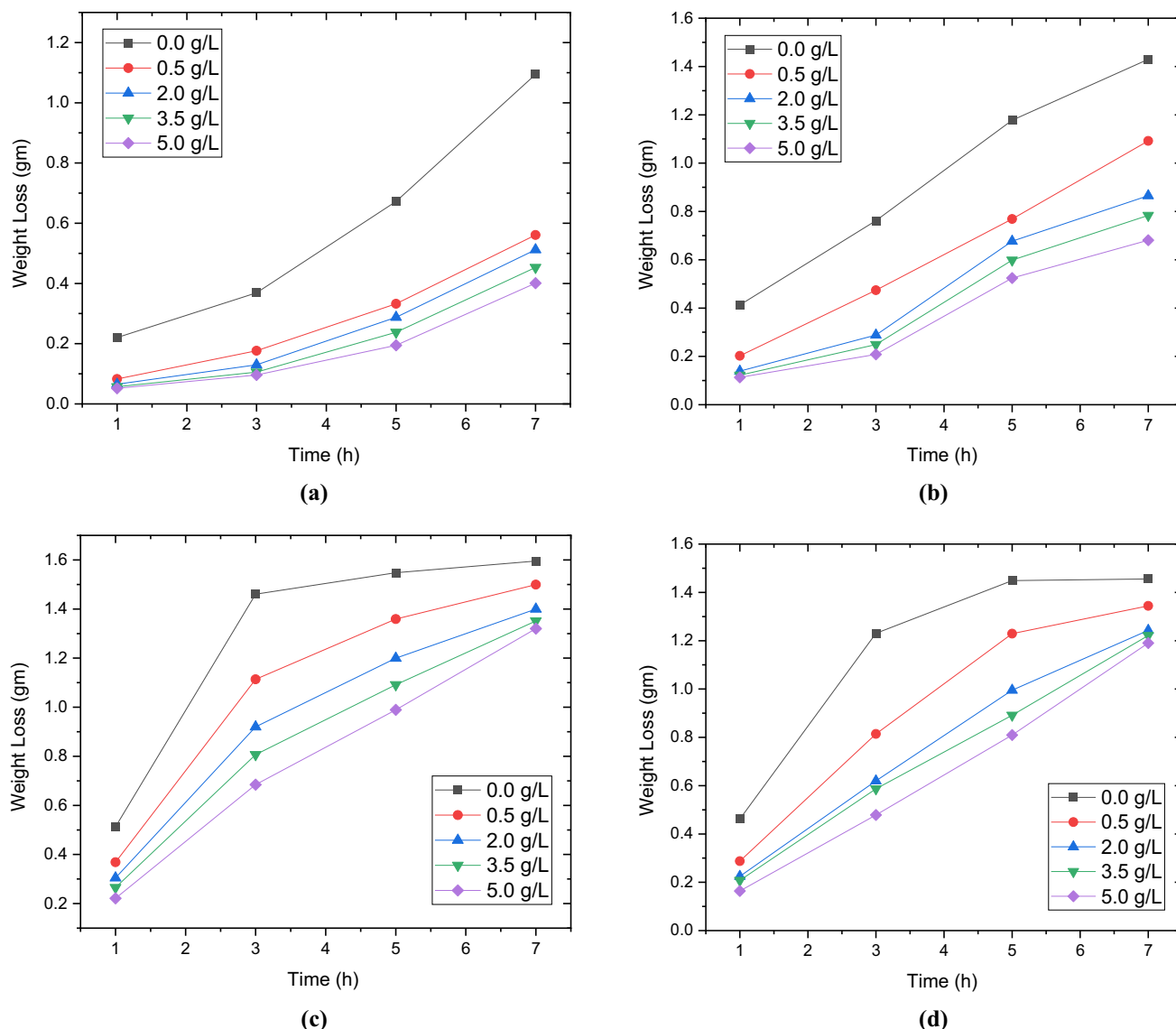**Fig. 4** Weight loss of EN8 steel at a different time of exposure and temperature (without inhibitor)

Fig. 5 Weight loss data of EN8 steel in 0.5 M H_2SO_4 with pectin at **a** 40 °C, **b** 50 °C, **c** 60 °C and **d** 70 °C temperature

loss and increases inhibition efficiency as the inhibitor concentration increased.

Effect of corrosion process with temperature and calculations of activation parameters

Figure 6 shows the effect of weight loss at different immersion times and various temperatures for various pectin concentrations. There was an increase in the weight loss for both the conditions due to deterioration of efficiency at higher exposure time and physical adsorption of inhibitor is indicated with a reduction in efficiency with increase in temperature. There is the electrostatic interaction between pectin molecules and the surface of the metal. These electrostatic interactions between the inhibitor and the metallic

surface decrease their attractive strength with increasing temperatures.

Arrhenius plot [ln (CR) vs $1/T$] and ln (CR/T) vs $1/T$ in 0.5 M H_2SO_4 comprising various concentrations of pectin at 1 h immersion time for EN8 DP steel with F-M structure is presented in Fig. 7. The activation parameters for the deterioration of EN8 steel in 0.5 M H_2SO_4 comprising pectin are presented in Table 2. As inhibitor concentrations increase, activation energy (E_a) has increased, indicating that the energy barrier increases as pectin concentration increases (Prabhu et al. 2021). Activation enthalpy ($\Delta H^{\#}$) values vary depending on E_a, indicating the recommended mechanism. The activation values of entropy ($\Delta S^{\#}$) were negative, which symbolizes the association of the molecules and the decrease in the disorder during the formation
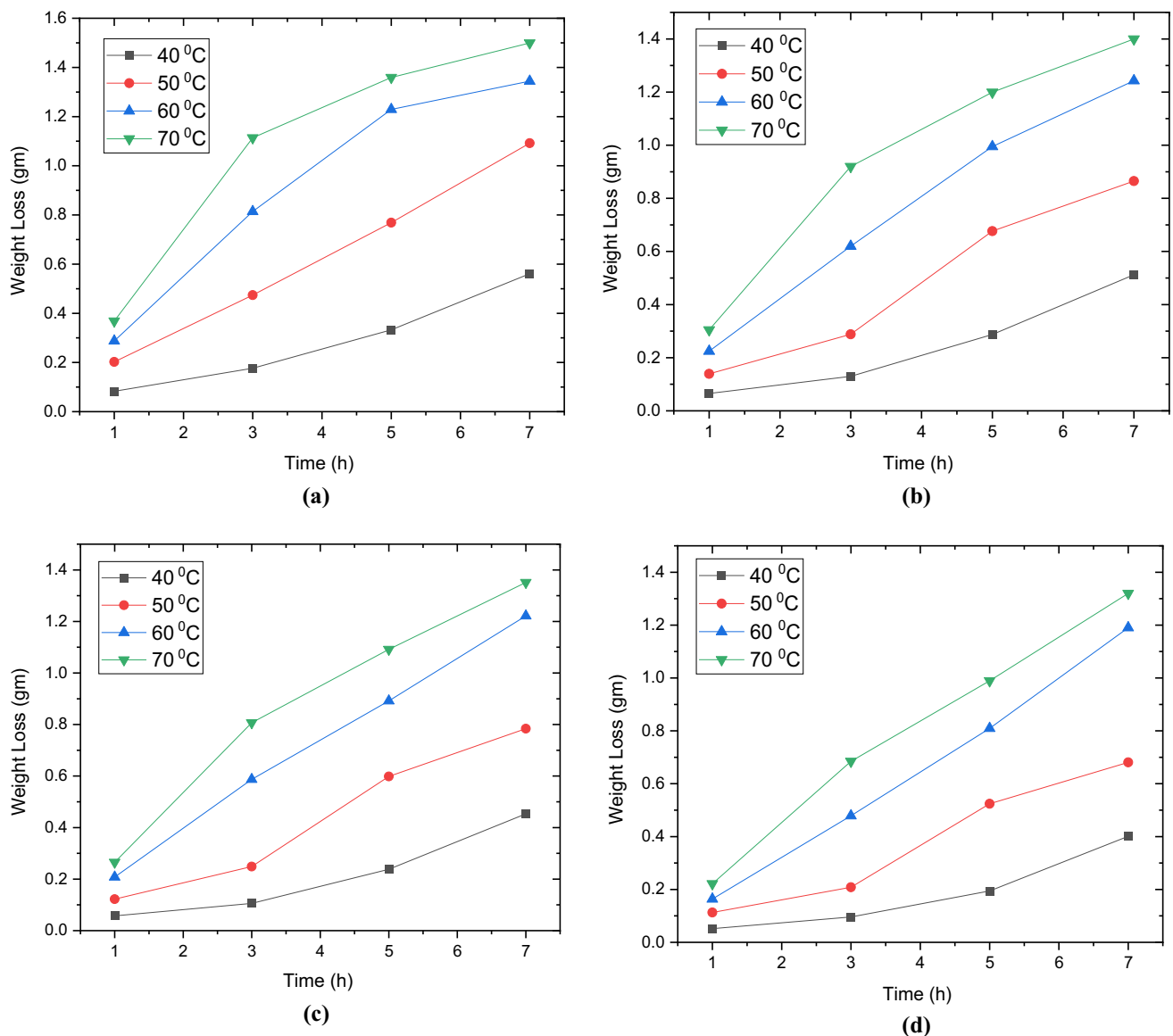
Fig. 6 Weight loss data of EN8 steel in 0.5 M H$_2$SO$_4$ at various temperatures and at **a** 0.5 g/L, **b** 2.0 g/L, **c** 3.5 g/L and **d** 5.0 g/L pectin concentration

of the activated complex (Oguzie et al. 2008; Prabhu et al. 2021).

Adsorption isotherm and thermodynamic parameters

Pectin adsorption on EN8 steel with DP structure F-M in 0.5 M H$_2$SO$_4$ followed the Langmuir adsorption isotherm, shown in Fig. 8a. The standard free adsorption energy ($\Delta G°_{ads}$) is provided by the adsorption equilibrium constant (K) (Akinbulumo et al. 2020; Prabhu et al. 2021). A graph of $\Delta G°_{ads}$ with T for pectin on EN8 steel with DP structure

F-M in 0.5 M H$_2$SO$_4$ is given in Fig. 8b. The thermodynamic factors for the absorption of pectin are presented in Table 3.

With pectin as an inhibitor, the $\Delta G°_{ads}$ was less than −20 kJ/mol (Galo et al. 2020) and the value increased with the increase in T, which proposed physical adsorption of pectin on the surface of the metal (Fouda et al. 2009). The negative value of the adsorption enthalpy ($\Delta H°_{ads}$) indicated the exothermal process, which also confirms physisorption. The high and negative value of adsorption entropy ($\Delta S°_{ads}$) represents the systematic placement of inhibitory molecules on the surface (Tang et al. 2003).
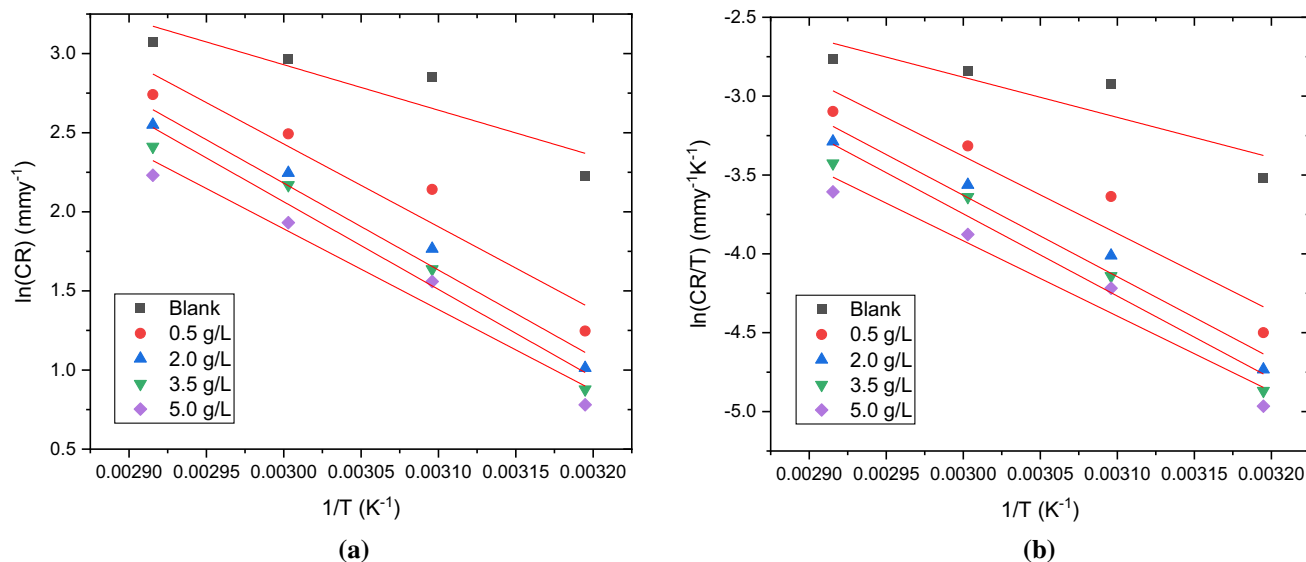
Fig. 7 Arrhenius plot and graph of ln (CR/T) versus $1/T$ for DP EN8 F-M steel in 0.5 M H$_2$SO$_4$ comprising various concentrations of pectin at 1 h immersion time

Table 2 Activation parameters for the corrosion of EN8 steel in 0.5 M H$_2$SO$_4$ with various pectin concentrations

Time	[Pectin] (g/L)	E_a (kJ/mol)	$\Delta H^{\#}$ (kJ/mol)	$\Delta S^{\#}$ (J/mol/K)
1 h	0.0	23.90	21.18	− 157.98
	0.5	43.47	40.75	− 103.43
	2.0	45.65	42.93	− 98.95
	3.5	46.06	43.34	− 98.68
	5.0	42.40	39.68	− 111.11
3 h	0.0	41.38	38.66	− 98.06
	0.5	54.46	51.75	− 62.06
	2.0	59.45	56.73	− 49.48
	3.5	62.36	57.52	− 41.73
	5.0	60.24	59.64	− 49.52
5 h	0.0	24.43	21.71	− 147.19
	0.5	42.25	39.53	− 95.75
	2.0	42.03	39.31	− 97.69
	3.5	44.70	41.98	− 90.62
	5.0	47.83	45.11	− 82.15
7 h	0.0	10.35	7.63	− 188.68
	0.5	28.47	25.75	− 135.60
	2.0	30.35	27.63	− 130.84
	3.5	33.44	30.72	− 121.98
	5.0	37.10	34.38	− 111.46

Open circuit potential (OCP) and Potentiodynamic polarization measurements

Figure 9 shows the difference of the open circuit potential (OCP) with time for EN8 steel corrosion against 0.5 M H$_2$SO$_4$ solution in the presence and absence of pectin. The inclusion of an inhibitor in the sulphuric acid medium led to a positive shift in OCP versus blank potential. This is due to a delay in anodic reaction. The slight positive variation in potential over time is due to the formation of corrosion products and/or an inhibitor film on the surface of the metal that offered partial protection of the material.

The corrosion of EN8 steel was carried out in 0.5 M H$_2$SO$_4$ and with different pectin concentrations at 40 °C. Figure 10 shows the potentiodynamic plots for the corrosion of EN8 DP steel in 0.5 M H$_2$SO$_4$ with different pectin concentrations at 40 °C. The anodic slopes of Tafel (β_a) and the cathodic slope of Tafel (β_c) obtained showed no substantial variation in values, indicated that there was no change in the mechanics of the anodic and cathodic process of pectin. The difference of E$_{corr}$ values between the blank and inhibited solution was not more than ± 85 mV (Nathan 1973) suggesting that pectin acts as a mixed type of inhibitor. The i$_{corr}$ values decreased with increased pectin concentration indicating increased effectiveness of pectin inhibition. Results obtained from PDP on EN8 DP steel with F-M structure containing pectin at 40 °C are given in Table 4.

EIS method

The Nyquist plots for the corrosion of EN8 steel with F-M DP structure were performed in 0.5 M H$_2$SO$_4$ and with various amounts of pectin at 40 °C are given in Fig. 11.

The Nyquist plots displayed a high-frequency (HF) capacitive loop indicating the Faradic process at the electrode sites. HF loops can be credited on the charge transfer process
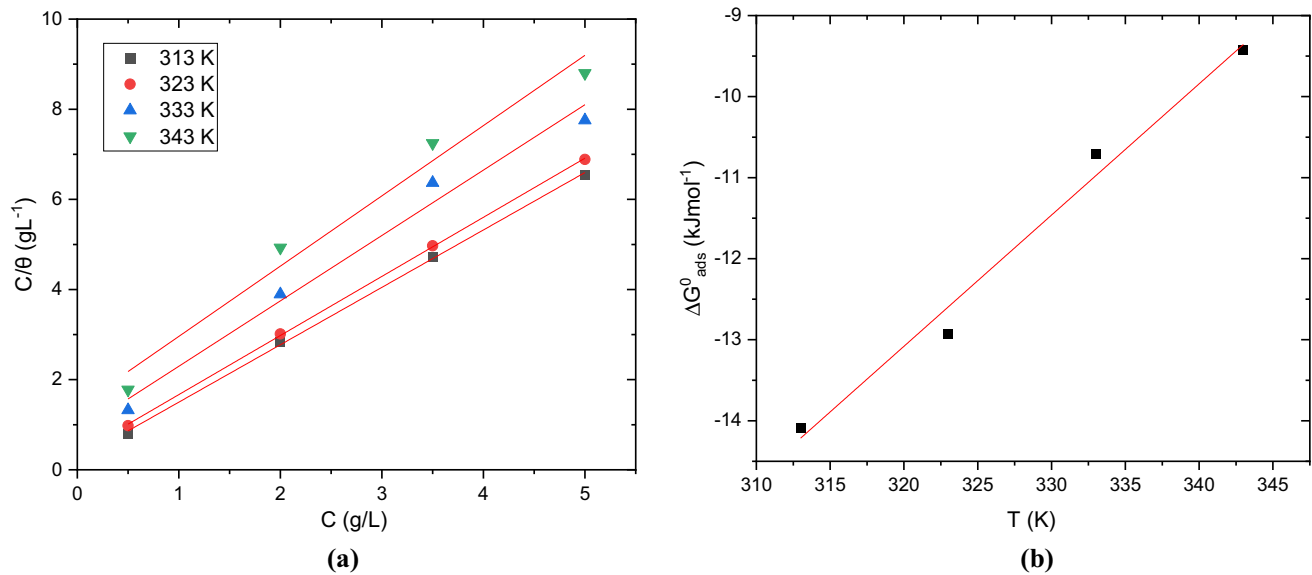
Fig. 8 **a** Langmuir adsorption isotherm and **b** Graph of adsorption free energy compared to T for pectin in 0.5 M H$_2$SO$_4$ for corrosion of EN8 steel during at 1 h immersion time

Table 3 Thermodynamic parameters for pectin adsorption to EN8 steel in 0.5 M H$_2$SO$_4$ at various temperatures

Time	Temp (K)	ΔG°_{ads} (kJ/mol)	ΔH°_{ads} (kJ/mol)	ΔS°_{ads} (J/mol/K)
1 h	313	− 14.0836	− 64.90	− 161.94
	323	− 12.9229		
	333	− 10.7127		
	343	− 9.4223		
3 h	313	− 12.6030	− 49.22	− 117.23
	323	− 11.0780		
	333	− 10.5005		
	343	− 8.8877		
5 h	313	− 11.7881	− 65.76	− 172.39
	323	− 10.3844		
	333	− 7.8275		
	343	− 6.8939		
7 h	313	− 12.1600	− 82.82	− 227.11
	323	− 9.1790		
	333	− 6.5089		
	343	− 5.4794		

Fig. 9 OCP plots in 0.5 M H$_2$SO$_4$ comprising various concentrations of pectin at 40 °C for corrosion of EN 8 steel using saturated calomel electrode (SCE) as the reference electrode

Nyquist plotted and the C_{dl} can be computed using the Eq. 5 (Machnikova et al. 2008; Toppo et al. 2013).

$$C_{dl} = Q(\omega_{max})^{n-1}, \tag{5}$$

where Q, CPE; ω_{max}, maximum impedance rate and n, CPE exponent. The slight change in capacity relative to its actual value was calculated using Eq. 6.

and the time constant of the dual electric layer (Cesiulis et al. 2016).

The equivalent circuit is comprised of the constant phase element (CPE) [from which double-layer capacitance (C_{dl}) is calculated using Eq. 5 & 6] parallel to the charge transfer resistance (R_{ct}) [from which R$_p$ is calculated using Eq. 7].

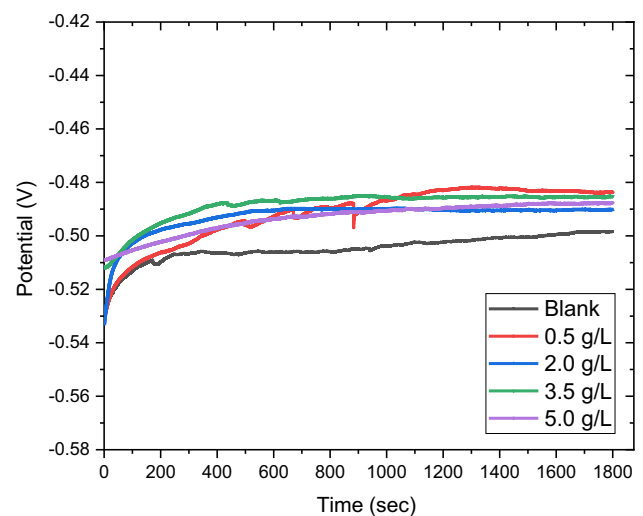A C_{dl} is replaced by a CPE (Q) in the circuit used is to take into account the depressed capacitive nature of
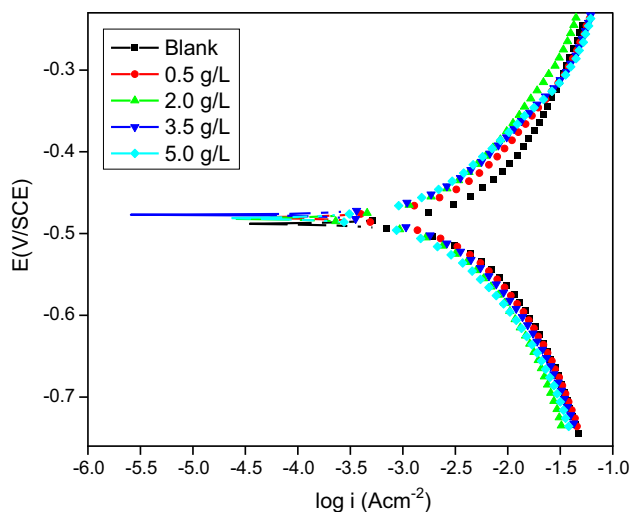
Fig. 10 PDP graphs in 0.5 M H_2SO_4 comprising different pectin concentrations at 40 °C for corrosion of EN8 steel

$$C_{dl} = \frac{1}{2\pi f_{max} R_p},$$ (6)

f_{max} = maximum frequency at which the imaginary component. The polarization resistance (R_P) was calculated using Eq. 7.

$$R_p = R_s + R_{ct}$$ (7)

The results of the regression calculations for this system are illustrated in Fig. 12, obtained by fitting the experimental data in the ZSimpWin software to the relevant equivalent circuit model. Impedance parameters such as charge transfer resistance (R_{ct}), double-layer capacitance (C_{dl}), and inhibition efficiency (IE$_{EIS}$ %) are given in Table 5.

From the results, it is seen that the value of R_p was increasing with increased pectin concentration and C_{dl} was decreasing. This is due to the absorption of pectin molecules on the surface of EN8 steel forming a physical barrier between the metal and the corrosive medium. The dielectric constant decreases and the thickness of the double layer at the metal and electrolyte interface increases, resulting in a decrease in the capacitance of the double electric layer (C_{dl}).

The IE% obtained from the EIS measurements was in agreement with that obtained from the PDP technique.

Bode plots depict the nature of the electrochemical system according to frequency. Figure 13 presents the Bode graph for DP EN8 steel in the absence and presence of different pectin concentrations. The increase in the phase angle with the increase in pectin concentrations is attributable to the decrease in metallic corrosion. This is due to the reduction of capacitive behavior at the metal–inhibitor interface. In the Bode magnitude graph, only one slope was found for the corrosion and inhibition process. The Bode plots signify that the difference between the HF limit and LF limit corresponds to the Rp (Pais and Rao 2020) values.

Surface characterization

Scanning electron microscopy (SEM) analysis

In Fig. 14a, the metal surface appears to be very smooth and even, with few scratches due to polishing. Figure 14b shows the EN8 steel metallic surface in contact with 0.5 M H_2SO_4 for 3 h. The material undergoes severe corrosion of DP EN8
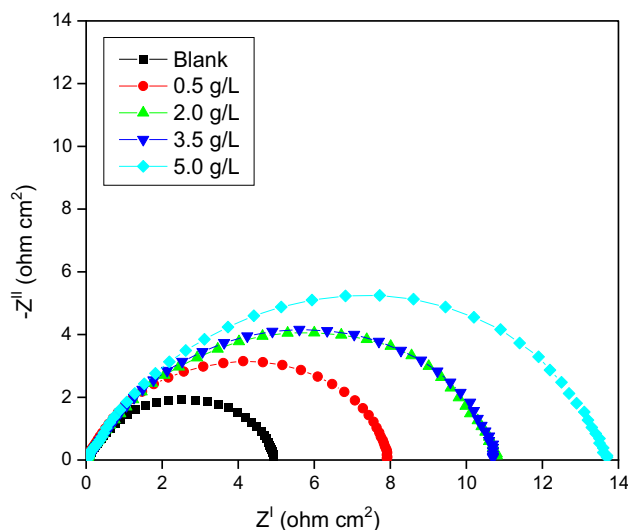

Fig. 11 Nyquist plots in 0.5 M H_2SO_4 comprising various pectin concentrations at 40 °C for corrosion of DP F-M EN8 steel

Table 4 Results of PDP measurements for corrosion of EN8 steel in 0.5 M H_2SO_4 containing various concentrations of pectin at 40 °C	[Pectin] (g/L)	E_{corr} (mV vs SCE)	i_{corr} (mA cm^{-2})	$-\beta_c$ (m V dec^{-1})	β_a (m V dec^{-1})	IE (%)
	0.0	−491	4.413	588	605	–
	0.5	−488	2.733	630	656	38.06
	2.0	−482	2.269	644	676	48.58
	3.5	−477	2.153	690	766	51.20
	5.0	−481	1.650	723	819	62.60

Fig. 12 Equivalent circuit fit with experimental data using ZSimpWin software
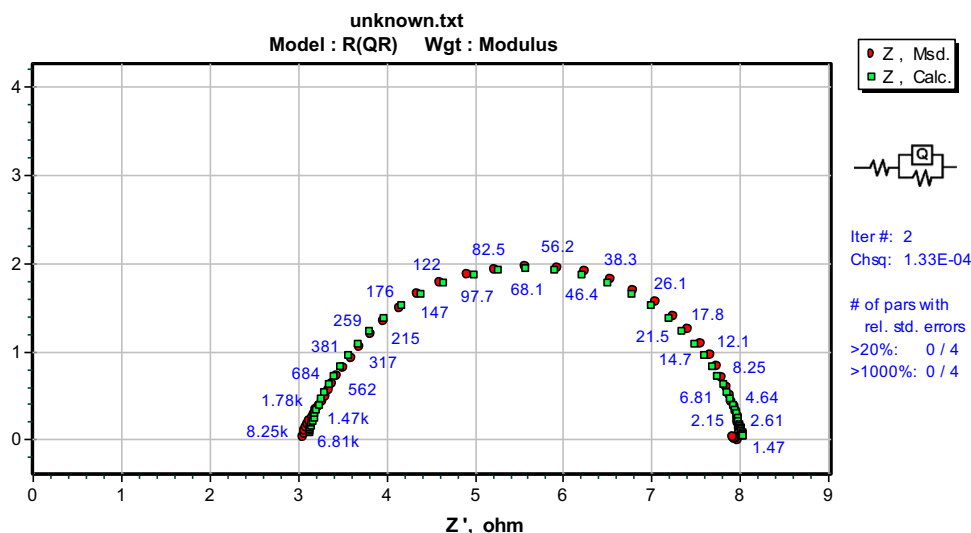

Table 5 Results of EIS measurements for corrosion of DP EN8 steel in 0.5 M H_2SO_4 comprising various pectin concentrations at 40 °C

[Pectin] (g/L)	R_s (Ω cm^2)	CPE ($\times 10^{-3}$)	n	R_{ct} (Ω cm^2)	R_p (Ω cm^2)	C_{dl} (μ F cm^{-2})	IE (%)
0.0	3.105	1.181	0.8485	4.941	8.046	98.85	–
0.5	2.649	0.995	0.8469	7.989	10.638	46.77	24.36
2.0	2.413	1.202	0.7897	13.13	15.543	25.61	48.23
3.5	3.341	1.041	0.7899	13.08	16.421	23.08	51.00
5.0	2.579	1.015	0.8096	13.98	19.259	15.03	58.22
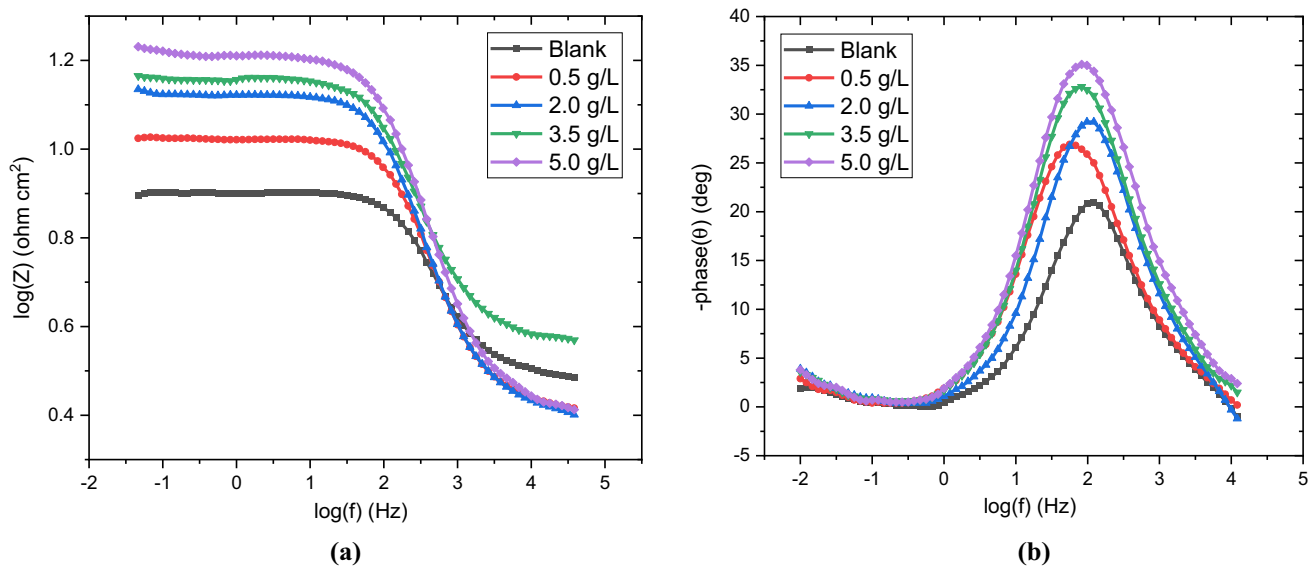
Fig. 13 **a** Bode magnitude plots and **b** Bode phase plots for control of corrosion of DP EN8 steel in the absence and presence of various concentrations of pectin at 40 °C in 0.5 M H2SO4

steel in the selected medium which is observed in the SEM image. The surface of the corroded specimen is very uneven as a result of the dissolution of the metal and the deposition of the corrosion product. In certain areas, there are pits.
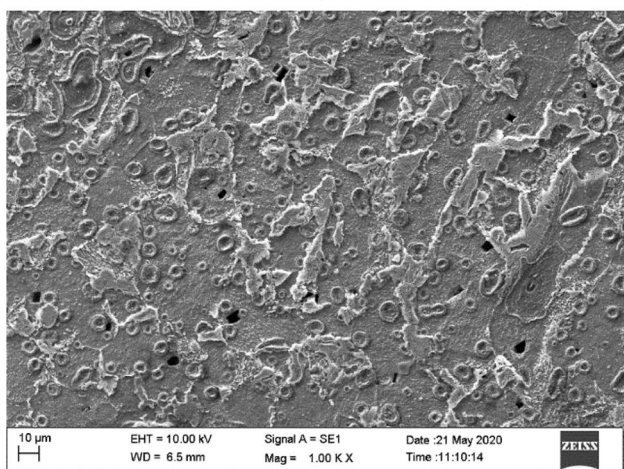
Cavity formation may be caused by the separation of the corrosion product from the metal. Adding 5.0 g/L of pectin revealed a remarkable change in the surface of the metal (Fig. 14 c). The added inhibitor was capable of covering
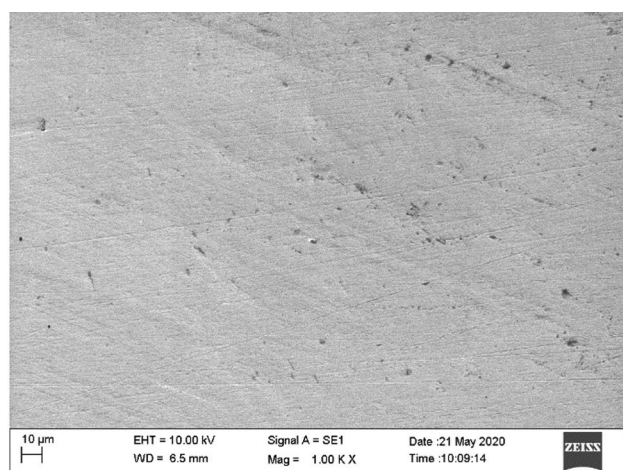
(a)
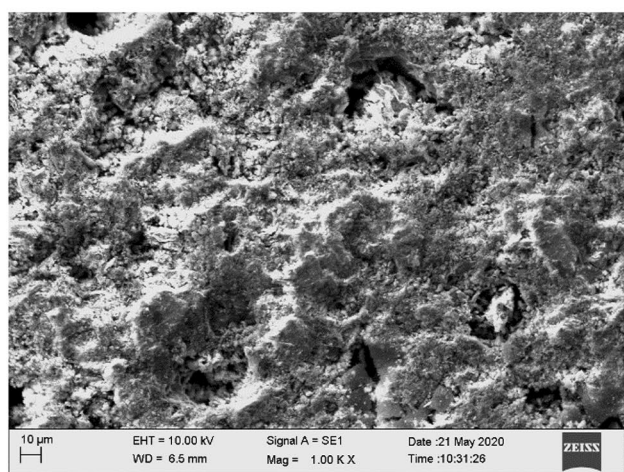
(b)

(c)

Fig. 14 SEM images of **a** freshly polished, **b** EN8 steel + 0.5 M H₂SO₄, **c** EN8 steel + 0.5 M H₂SO₄ + 5.0 g/L pectin

almost all cavities of the surface, forming a barrier between the metal and the medium, preventing corrosion.

Energy dispersive X-ray (EDX) analysis

The EDX spectra were taken for polished, corroded, and inhibited samples. The images of the spectra are shown in Fig. 15 along with its elemental analysis. The presence of a large amount of percentage of oxygen is observed in the corroded sample. This is due to the formation of the metal oxide layer. In the presence of 5.0 g/L pectin, there is an increase in the percentage composition of carbon and decreased concentration of oxygen. This confirmed the adsorption of pectin on the surface of the metal thereby successfully decreases the corrosion. Now, the presence of oxygen after inhibition is due to the OH groups present on pectin.

Atomic force microscopy (AFM) analysis

The 3D images of DP EN8 steel for the freshly polished, sample dipped in 0.5 M H₂SO₄ along with the 5.0 g/L pectin are presented in Fig. 16a–c, respectively. The values such as average surface roughness (R_a), root mean square roughness (R_q), and R$_{max}$ values derived from AFM studies are provided in Table 6. It is clear from the results of R_a, R_q, and (P–V) that for the inhibited sample, the values are much lower than in the absence of pectin (Pais and Rao 2020). This is a clear indication of the adsorbed pectin on the surface of the EN8 steel.

X-ray diffraction technique (XRD) analysis

XRD was utilized to study the formation of pectin film on DP EN8 steel. XRD spectra were recorded for the EN8 steel and EN8 steel + 5.0 g/L pectin by dipping in 0.5 M H₂SO₄ for 24 h. The DP EN8 steel in the presence of 0.5 M H₂SO₄ underwent corrosion produces peaks at $2\theta = 44.70°$, and 64.92° (Fig. 17a) due to iron oxides (Fe_3O_4 and FeOOH). The XRD spectra of the DP EN8 steel surface submerged in the 0.5 M H₂SO₄ acid solution comprising 5.0 g/L of pectin are shown in Fig. 17b. The high peak intensity observed around 45° at 2θ is linked to the Fe phase and the iron oxide peaks are significantly reduced. This change in peaks of inhibited surface suggests a layer formed on the surface of the metal. The results also signify the possibility of pectin film formation on the surface of the metal.
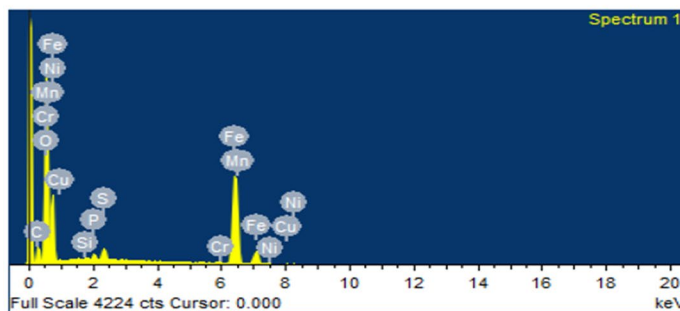
Corrosion inhibition mechanism

Pectin reacts with the sulphuric acid solution in the corrosive. Because of this, they become cations, existing in equilibrium with the corresponding molecular shape.

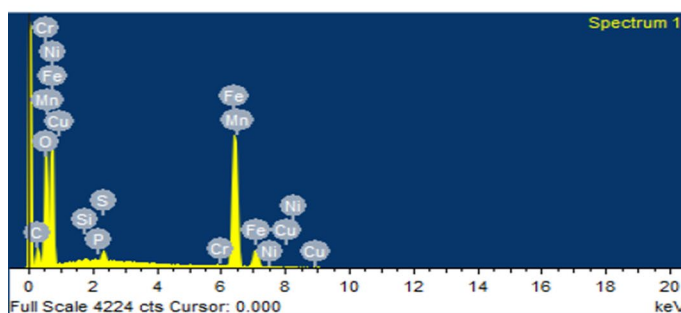**Fig. 15** EDX spectra of **a** freshly polished, **b** EN8 steel + 0.5 M H_2SO_4 **(c)** EN8 steel + 0.5 M H_2SO_4 + 5.0 g/L pectin
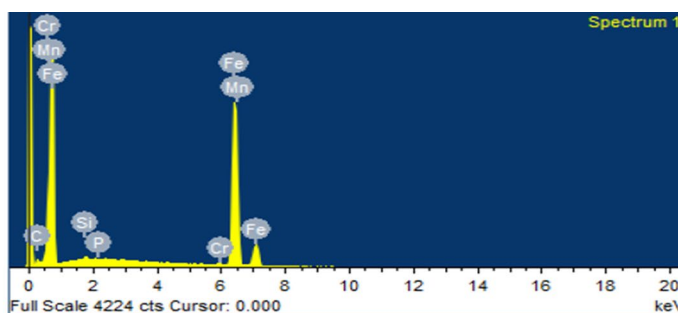
Element	Weight %
C	2.43
Si	0.28
P	0.15
Cr	0.14
Mn	0.70
Fe	96.30

(a)

Element	Weight %
C	6.76
O	32.25
Si	0.11
P	0.68
S	1.29
Cr	0.10
Mn	0.73
Fe	56.47
Ni	0.68
Cu	0.94

(b)

Element	Weight%
C	7.20
O	19.35
Si	0.12
P	0.14
S	0.95
Cr	0.17
Mn	0.48
Fe	70.87
Ni	0.28
Cu	0.44

(c)

$$PECTIN - OH + xH^+ \rightarrow [PECTIN - OHH_x]^{x+} \qquad (8)$$

Physical adsorption can occur due to electrostatic interaction among protonated pectin molecules with the sulfate ion-covered metal surface. Interaction between electrons of oxygen of OH group with the metallic surface may also take place. Chemical adsorption occurs due to the result of π-orbitals interaction with the metallic surface, this is not happing because there are very few π bonds (C = O) usually placed away from the metal surface as indicated in Fig. 18. In the present study, the free energy of adsorption values is lower than the − 20 kJ/mol, therefore, shows that the adsorption of pectin molecules at the surface of DP EN8 steel is primarily by physical adsorption.

Conclusions

In this study, the effect of DP EN8 F-M steel exposed to 0.5 M H_2SO_4 solution was studied by immersion corrosion and electrochemical measurements. From the results of the experiments, the following conclusions were arrived at.

- From the weight loss study, highest inhibition efficiency of 76.43% was achieved at 5.0 g/L at 1 h of exposure at 40 °C.
- The inhibition efficiency increases with increased inhibitor concentration and decreases with temperature.
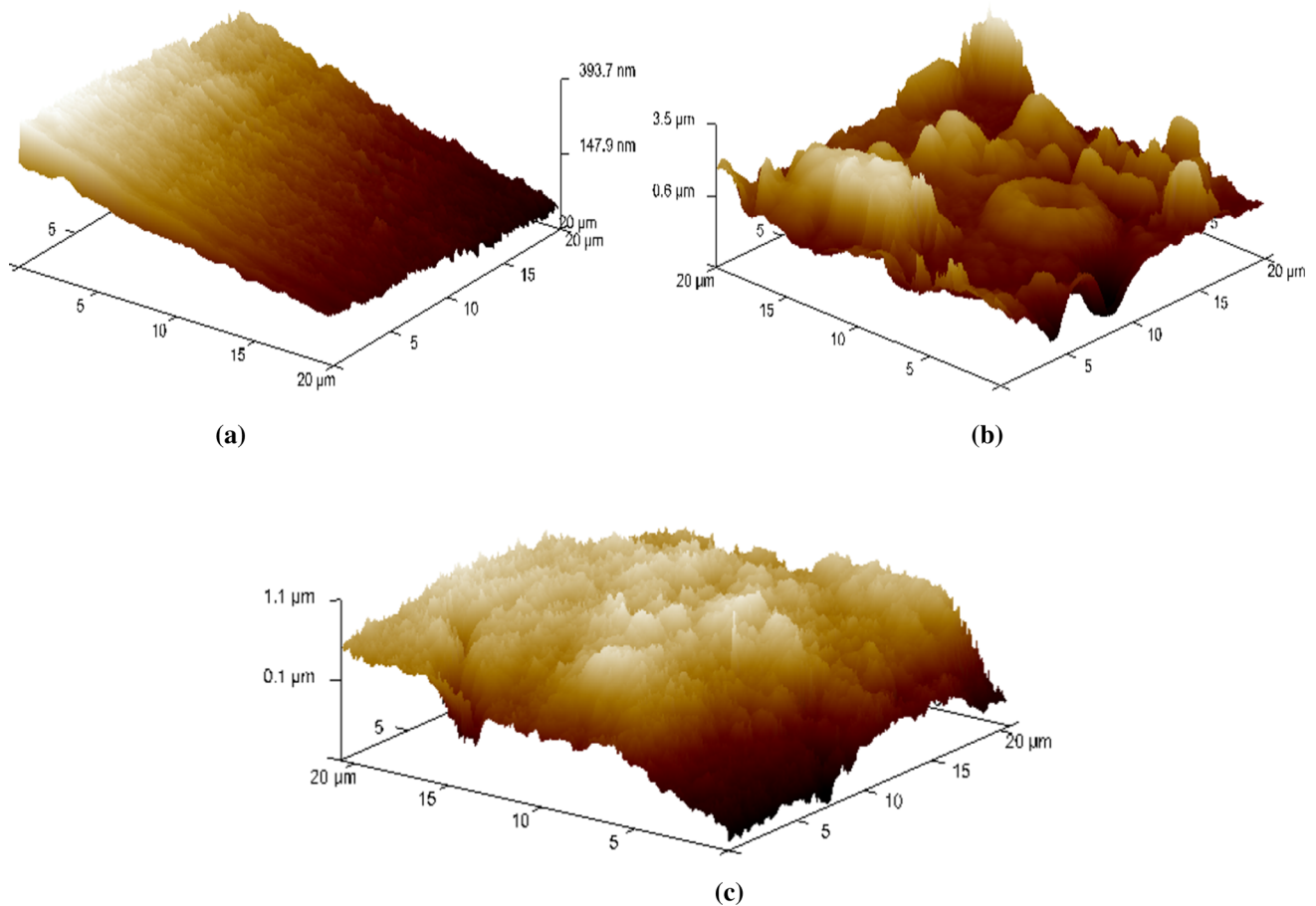
Fig. 16 AFM spectra of **a** freshly polished, **b** EN8 steel + 0.5 M H$_2$SO$_4$, **c** EN8 steel + 0.5 M H$_2$SO$_4$ + 5.0 g/L pectin

Table 6 AFM data obtained for DP EN8 steel in 0.5 M H$_2$SO$_4$

Samples	R_a (nm)	R_q (nm)	R_{max} (nm)
Freshly polished DP EN8 steel	50	80	951
EN8 steel + 0.5 M H$_2$SO$_4$	478	403	3156
EN8 steel + 0.5 M H$_2$SO$_4$ + 5.0 g/L pectin	195	254	1846

- The inhibitor acts as a mixed inhibitor at the surface of EN8 steel with a dual-phase F-M structure.
- The pectin is physically adsorbed onto the surface of the DP EN8 steel with an F-M structure and obeys the Langmuir adsorption isotherm.
- The corrosion control of DP EN8 steel with F-M structure in 0.5 M sulphuric acid solution with pectin with

Fig. 17 XRD spectrum of DP EN8 steel corrosion in 0.5 M H$_2$SO$_4$ **a** Blank (Blue) and **b** presence of pectin (Red)
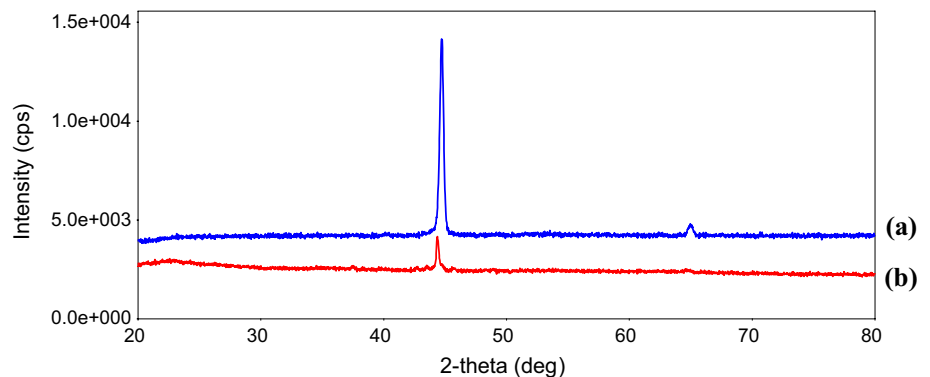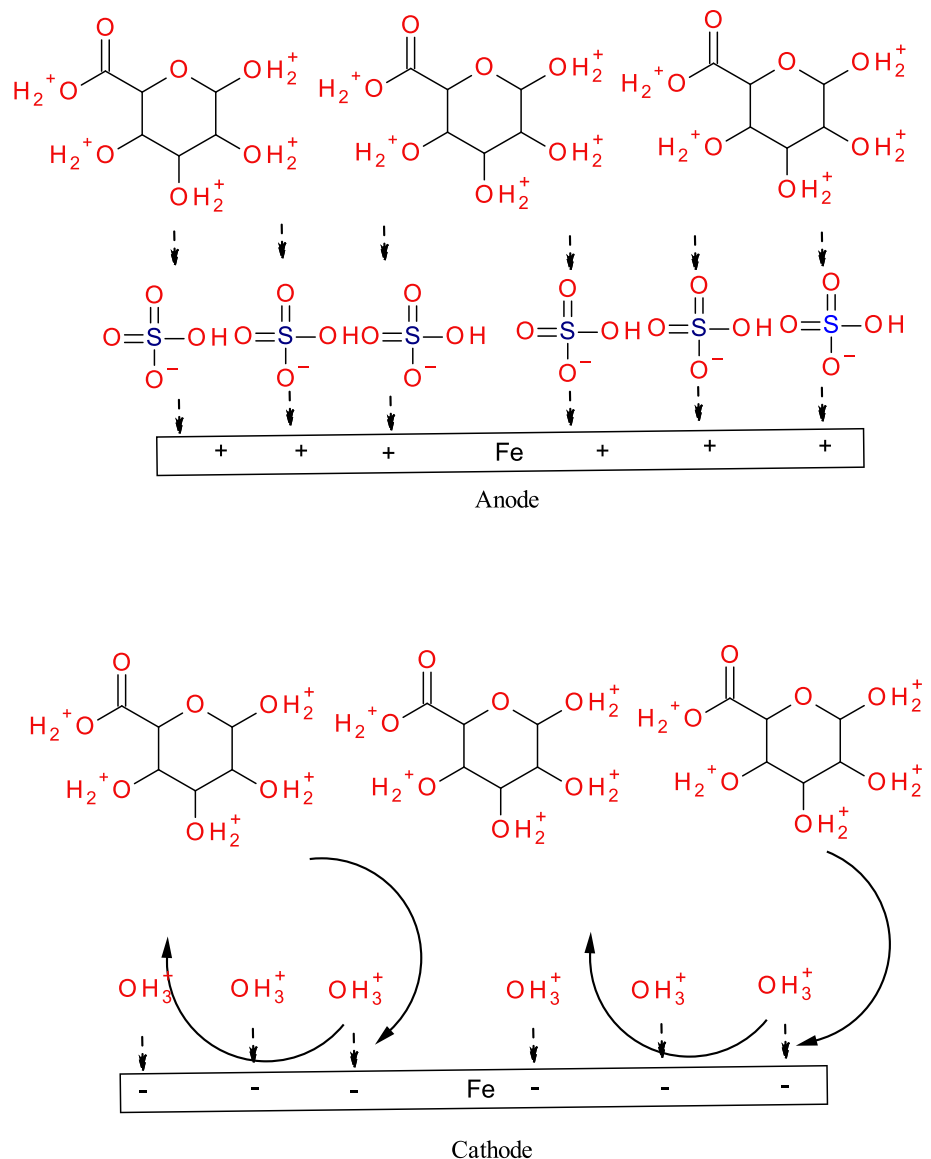
Fig. 18 Schematic representation of the absorption of pectin at the surface of the anodic and cathodic zone of the metal

Anode

Cathode

an efficiency of 62% was obtained with 5.0 g/L of pectin at 40 °C.

- Thus, pectin is a good, renewable, easy to find, cost-effective, and environmentally safe inhibitor.

Declarations

References

ASTM G1-03 (2017) Standard practice for preparation, cleaning, and evaluating corrosion test specimens. ASTM Standard. http://www.astm.org/cgi-bin/resolver.cgi?G1-03

Abedini O, Behroozi M, Marashi P, Ranjbarnodeh E, Pouranvari M (2019) Intercritical heat treatment temperature dependence of mechanical properties and corrosion resistance of dual phase steel. Mater Res 22:1–10

Akinbulumo OA, Odejobi OJ, Odekanle EL (2020) Thermodynamics and adsorption study of the corrosion inhibition of mild steel by *Euphorbia heterophylla* L. extract in 1.5 M HCl. Results in Materials 5:100074. https://doi.org/10.1016/j.rinma.2020.100074

Basantia SK, Bhattacharya A, Khutia N, Das D (2021) Plastic behavior of ferrite-pearlite, ferrite-bainite and ferrite–martensite steels: experiments and micromechanical modelling. Met Mater Int 27:1025. https://doi.org/10.1007/s12540-019-00519-5

Bentiss F, Lebrini M, Lagrenée M (2005) Thermodynamic characterization of metal dissolution and inhibitor adsorption processes in mild steel/2,5-bis(n-thienyl)-1,3,4-thiadiazoles/hydrochloric acid system. Corros Sci 47(12):2915–2931. https://doi.org/10.1016/j.corsci.2005.05.034

Berradja A (2019) Electrochemical techniques for corrosion and tribocorrosion monitoring: methods for the assessment of corrosion rates. Corros Inhib. https://doi.org/10.5772/intechopen.86743

Bignozzi MC, Calcinelli L, Carati M, Ceschini L, Chiavari C, Masi G, Morri A (2020) Effect of heat treatment conditions on retained austenite and corrosion resistance of the X190CrVMo20-4-1 stainless steel. Met Mater Int 26(9):1318–1328. https://doi.org/10.1007/s12540-019-00384-2

Bilal MM, Yaqoob K, Zahid MH, Haq EU, Tanveer WH, Wadood A, Ahmed B (2019) Effect of austempering conditions on the microstructure and mechanical properties of AISI 4340 and AISI 4140 steels. J Market Res 8(6):5194–5200. https://doi.org/10.1016/j.jmrt.2019.08.042

Branzoi F, Băran A, Ludmila A, Alexandrescu E (2020) The inhibition action of some organic polymers on the corrosion carbon steel in acidic media. Chem Pap 74(12):4315–4335. https://doi.org/10.1007/s11696-020-01242-x

Cesiulis H, Tsyntsaru N, Ramanavicius A, Ragoisha G (2016) The study of thin films by electrochemical impedance spectroscopy. In: Tiginyanu I, Topala P, Ursaki V (eds) Nanostructures and thin films for multifunctional applications. NanoScience and Technology. Springer, Cham. https://doi.org/10.1007/978-3-319-30198-3_1

Charitha BP, Rao P (2020) Pectin as a potential green inhibitor for corrosion control of 6061Al–15%(V) SiC(P) composite in acid medium: electrochemical and surface studies. J Fail Anal Prev 20(5):1684–1696. https://doi.org/10.1007/s11668-020-00973-z

El Faydy M, Lakhrissi B, Jama C, Zarrouk A, Olasunkanmi LO, Ebenso EE, Bentiss F (2020) Electrochemical, surface and computational studies on the inhibition performance of some newly synthesized 8-hydroxyquinoline derivatives containing benzimidazole moiety against the corrosion of carbon steel in phosphoric acid environment. J Market Res 9(1):727–748. https://doi.org/10.1016/j.jmrt.2019.11.014

Fereiduni E, Ghasemi Banadkouki SS (2014) Improvement of mechanical properties in a dual-phase ferrite–martensite AISI4140 steel under tough-strong ferrite formation. Mater Des 1980–2015(56):232–240. https://doi.org/10.1016/j.matdes.2013.11.005

Fischer H, Karlsruhe (1974) Corrosion Inhibitors. Herausgeber: *C. C. Nathan*, 284 Seiten, gebunden, October 1973. National Association of Corrosion Engineers, P.O. Box 1499, Houston, Tx 77001. Preis: 30 Dollar. Materials and Corrosion, vol. 25. pp 803–804. https://doi.org/10.1002/maco.19740251032

Fouda AS, Al-Sarawy AA, Ahmed FS, El-Abbasy HM (2009) Corrosion inhibition of aluminum 6063 using some pharmaceutical compounds. Corros Sci 51(3):485–492. https://doi.org/10.1016/J.CORSCI.2008.10.012

Galo GT, Morandim-Giannetti AdeA, Cotting F, Aoki IV, Aquino IP (2020) Evaluation of purple onion (*Allium cepa* L.) extract as a natural corrosion inhibitor for carbon steel in acidic media. Metals Mater Int. https://doi.org/10.1007/s12540-020-00679-9

Gerengi H, Sen N, Uygur I, Kaya E (2020) Corrosion behavior of dual phase 600 and 800 steels in 3.5 wt.% NaCl environment. J Adhes Sci Technol 34(8):903–915. https://doi.org/10.1080/01694243.2019.1688925

Gürkan Aydın AY (2019) Effect of quenching and tempering temperature on corrosion behavior of boron steels in 3.5 wt.% NaCl solution. Int J Electrochem Sci 14:2126–2135

Hoai NT, Van Hien P, Vu NSH, Son DL, Van Man T, Tri MD, Nam ND (2019) An improved corrosion resistance of steel in hydrochloric acid solution using Hibiscus sabdariffa leaf extract. Chem Pap 73(4):909–925. https://doi.org/10.1007/s11696-018-0649-6

Hynes NRJ, Selvaraj RM, Mohamed T, Mukesh AM, Olfa K, Nikolova MP (2021) Aerva lanata flowers extract as green corrosion inhibitor of low-carbon steel in HCl solution: an in vitro study. Chem Pap 75(3):1165–1174. https://doi.org/10.1007/s11696-020-01361-5

Karimi A, Kheirandish S, Mahmoudiniya M (2017) Effect of bainite volume fraction on mechanical properties of a ferrite-bainite-martensite steel. Kovove Mater 55(3):175–182

Katiyar PK, Misra S, Mondal K (2019) Comparative corrosion behavior of five microstructures (pearlite, bainite, spheroidized, martensite, and tempered martensite) made from a high carbon steel. Metall Mater Trans A 50(3):1489–1501. https://doi.org/10.1007/s11661-018-5086-1

Keleştemur O, Aksoy M, Yildiz S (2009) Corrosion behavior of tempered dual-phase steel embedded in concrete. Int J Miner Metall Mater 16(1):43–50. https://doi.org/10.1016/S1674-4799(09)60008-X

Kumar S, Kumar A, Vinaya R, Sah Madhusudhan R, Manjini S (2019) Mechanical and electrochemical behavior of dual-phase steels having varying ferrite–martensite volume fractions. J Mater Eng Perform 28(6):3600–3613. https://doi.org/10.1007/s11665-019-04101-3

Li X, Deng S, Lin T, Xie X, Du G (2019) Cassava starch ternary graft copolymer as a corrosion inhibitor for steel in HCl solution. J Market Res. https://doi.org/10.1016/j.jmrt.2019.12.050

Lowmunkhong P, Ungthararak D, Sutthivaiyakit P (2010) Tryptamine as a corrosion inhibitor of mild steel in hydrochloric acid solution. Corros Sci 52(1):30–36. https://doi.org/10.1016/j.corsci.2009.08.039

Ma J, Feng F, Yu B, Chen H, Fan L (2020) Effect of cooling temperature on the microstructure and corrosion behavior of X80 pipeline steel. Int J Miner Metall Mater 27(3):347–353. https://doi.org/10.1007/s12613-019-1882-x

Machnikova E, Whitmire KH, Hackerman N (2008) Corrosion inhibition of carbon steel in hydrochloric acid by furan derivatives. Electrochim Acta 53(20):6024–6032. https://doi.org/10.1016/j.electacta.2008.03.021

Mahgoub FM, Abdel-Nabey BA, El-Samadisy YA (2010) Adopting a multipurpose inhibitor to control corrosion of ferrous alloys in cooling water systems. Mater Chem Phys 120(1):104–108. https://doi.org/10.1016/j.matchemphys.2009.10.028

Manssouri M, Znini M, Lakbaibi Z, Ansari A, El Ouadi Y (2021) Experimental and computational studies of perillaldehyde isolated from Ammodaucus leucotrichus essential oil as a green corrosion inhibitor for mild steel in 1.0 M HCl. Chem Pap 75(3):1103–1114. https://doi.org/10.1007/s11696-020-01353-5

Mert BD, Mert ME, Kardaş G, Yazıcı B (2011) Experimental and theoretical investigation of 3-amino-1,2,4-triazole-5-thiol as a corrosion inhibitor for carbon steel in HCl medium. Corros Sci 53(12):4265–4272. https://doi.org/10.1016/j.corsci.2011.08.038

Negm NA, Kandile NG, Aiad IA, Mohammad MA (2011) New eco-friendly cationic surfactants: synthesis, characterization and applicability as corrosion inhibitors for carbon steel in 1N HCl. Colloids Surf A 391(1):224–233. https://doi.org/10.1016/j.colsurfa.2011.09.032

Obi-Egbedi NO, Obot IB, Umoren SA (2012) Spondias mombin L. as a green corrosion inhibitor for aluminium in sulphuric acid: Correlation between inhibitive effect and electronic properties of extracts major constituents using density functional theory. Arab J Chem 5(3):361–373. https://doi.org/10.1016/J.ARABJC.2010.09.002

Oguzie EE, Njoku VO, Enenebeaku CK, Akalezi CO, Obi C (2008) Effect of hexamethylpararosaniline chloride (crystal violet) on mild steel corrosion in acidic media. Corros Sci 50(12):3480–3486. https://doi.org/10.1016/j.corsci.2008.09.017

Pais M, Rao P (2020) Maltodextrin for corrosion mitigation of zinc in sulfamic acid: electrochemical, surface and spectroscopic studies. Int J Biol Macromol 145:575–585. https://doi.org/10.1016/j.ijbiomac.2019.12.197

Pais M, Rao P (2021) Electrochemical, spectroscopic and theoretical studies for acid corrosion of zinc using glycogen. Chem Pap 75(4):1387–1399. https://doi.org/10.1007/s11696-020-01391-z

Prabhu D, Rao P (2013) Coriandrum sativum L.—a novel green inhibitor for the corrosion inhibition of aluminium in 1.0 M phosphoric acid solution. J Environ Chem Eng 1(4):676–683. https://doi.org/10.1016/j.jece.2013.07.004

Prabhu D, Rao P (2019) A comparative study on inhibitory actions of TCE, GIE, and CSE on the corrosion of 6063 al alloy in H3PO4 medium. J Bio Tribo-Corros 5(3):76. https://doi.org/10.1007/s40735-019-0269-x

Prabhu PR, Prabhu D, Rao P (2020a) Analysis of Garcinia indica Choisy extract as eco-friendly corrosion inhibitor for aluminum in phosphoric acid using the design of experiment. J Market Res 9(3):3622–3631. https://doi.org/10.1016/j.jmrt.2020.01.100

Prabhu PR, Prabhu D, Sharma S, Kulkarni SM (2020b) Surface properties and corrosion behavior of turn-assisted deep-cold-rolled AISI 4140 STEEL. J Mater Eng Perform 29(9):5871–5885. https://doi.org/10.1007/s11665-020-05051-x

Prabhu D, Prabhu PR, Rao P (2021) Thermodynamics, adsorption, and response surface methodology investigation of the corrosion inhibition of aluminum by Terminalia chebula Ritz. extract in H3PO4. Chem Pap 75(2):653–667. https://doi.org/10.1007/s11696-020-01318-8

Qiang Y, Zhang S, Tan B, Chen S (2018) Evaluation of Ginkgo leaf extract as an eco-friendly corrosion inhibitor of X70 steel in HCl solution. Corros Sci 133:6–16. https://doi.org/10.1016/j.corsci.2018.01.008

Şahin EA, Solmaz R, Gecibesler İH, Kardaş G (2020) Adsorption ability, stability and corrosion inhibition mechanism of phoenix dactylifera extrat on mild steel. Mater Res Express 7(1):16585. https://doi.org/10.1088/2053-1591/ab6ad3

Salamci E, Candan S, Kabakci F (2017) Effect of microstructure on corrosion behavior of dual-phase steels. Kovove Mater 5(2):133–139

Saxena A, Sharma V, Thakur KK, Bhardwaj N (2020) Electrochemical studies and the surface examination of low carbon steel by applying the extract of citrus sinensis. J Bio Tribo-Corros 6(2):41. https://doi.org/10.1007/s40735-020-00338-x

Shahzad M, Tayyaba Q, Manzoor T, ud-din, R., Subhani, T., & Qureshi, A. H. (2018) The effects of martensite morphology on mechanical properties, corrosion behavior and hydrogen assisted cracking in A516 grade steel. Mater Res Express 5(1):16516. https://doi.org/10.1088/2053-1591/aaa55f

Shinato KW, Zewde AA, Jin Y (2020) Corrosion protection of copper and copper alloys in different corrosive medium using environmentally friendly corrosion inhibitors. Corros Rev 38(2):101–109. https://doi.org/10.1515/corrrev-2019-0105

Solomon MM, Umoren SA, Udosoro II, Udoh AP (2010) Inhibitive and adsorption behaviour of carboxymethyl cellulose on mild steel corrosion in sulphuric acid solution. Corros Sci 52(4):1317–1325. https://doi.org/10.1016/J.CORSCI.2009.11.041

Song D, Hao J, Yang F, Chen H, Liang N, Wu Y, Zhang J, Ma H, Klu EE, Gao B, Qiao Y, Sun J, Jiang J (2019) Corrosion behavior and mechanism of Cr–Mo alloyed steel: Role of ferrite/bainite duplex microstructure. J Alloys Compd 809:151787. https://doi.org/10.1016/j.jallcom.2019.151787

Song D, Wang G, Yang F, Chen H, Liang N, Ma H, Jiang J, Ma X (2020) Microstructure and deformation behavior of a novel steel rebar: Effect of the heterogeneous microstructure of soft ferrite and Hard bainite. J Market Res 9(6):12281–12292. https://doi.org/10.1016/j.jmrt.2020.08.085

Stoica M, Mikoliūnaitė L, Ramanavičienė A, Alexe P, Carac G, Dinica R, Voronovič J, Ramanavičius A (2012) Corrosion study of stainless steel incubated in solutions consisting of biocide (Oxonia-Active) and Aspergillus niger suspension. Chemija 23:180–186

Tabatabaei majd, M., Naderi, R., & Ramezanzadeh, B. (2020) Promotion of the active/barrier protection function of epoxy ester coating/steel system utilizing differently synthesized hybrid pigment through zinc acetylacetonate tailored with green inhibitor molecules. Prog Org Coat 138:105380. https://doi.org/10.1016/J.PORGCOAT.2019.105380

Tang L, Mu G, Liu G (2003) The effect of neutral red on the corrosion inhibition of cold rolled steel in 1.0 M hydrochloric acid. Corros Sci 45(10):2251–2262. https://doi.org/10.1016/S0010-938X(03)00046-5

Toppo A, Kaul R, Pujar MG, Kamachi Mudali U, Kukreja LM (2013) Enhancement of corrosion resistance of type 304 stainless steel through a novel thermo-mechanical surface treatment. J Mater Eng Perform 22(2):632–639. https://doi.org/10.1007/s11665-012-0304-2

Xiong Z, Kostryzhev AG, Zhao Y, Pereloma EV (2019) Microstructure evolution during the production of dual phase and transformation induced plasticity steels using modified strip casting simulated in the laboratory. Metals. https://doi.org/10.3390/met9040449

Zhang Q, Li Q, Chen X (2020) Effect of heat treatment on corrosion behavior of Mg–5Gd–3Y–0.5Zr alloy. RSC Adv 10(71):43371–43382. https://doi.org/10.1039/D0RA08933H

Zhao Z, Wang X, Qiao G, Zhang S, Liao B, Xiao F (2019) Effect of bainite morphology on deformation compatibility of mesostructure in ferrite/bainite dual-phase steel: mesostructure-based finite element analysis. Mater Des 180:107870. https://doi.org/10.1016/j.matdes.2019.107870

Zhu J, Sun X, Barber G, Han X, Qin H (2019) Effect of Carbon Content on Bainite Transformation Kinetics and Microstructure of 4140/4150 Steels. Eur Sci J 15(9):518–535. https://doi.org/10.19044/esj.2019.v15n9p518

Publisher's Note Springer Nature remains neutral with regard to jurisdictional claims in published maps and institutional affiliations.

Springer